JOURNAL OF PROPULSION AND POWER
Vol. 15, No. 6, November–December 1999

Steady-State Hydrazinium Nitroformate (HNF) Combustion Modeling

J. Louwers* and G. M. H. J. L. Gadiot†
TNO Prins Maurits Laboratory, 2280 AA Rijswijk, The Netherlands
M. Q. Brewster‡
University of Illinois at Urbana–Champaign, Urbana, Illinois 61801
S. F. Son§
Los Alamos National Laboratory, Los Alamos, New Mexico 87545
and
T. Parr¶ and D. Hanson-Parr¶
U.S. Naval Air Warfare Center, China Lake, California 93555-6001

Two simplified modeling approaches are used to model the combustion of hydrazinium nitroformate (HNF), $N_2H_5{\cdot}C(NO_2)_3$. The condensed phase is treated by high-activation-energy asymptotics. The gas phase is treated by two limit cases: the classical high-activation-energy approximation and the recently introduced low-activation-energy approach. This results in simplification of the gas-phase energy equation, making an (approximate) analytical solution possible. The results of both models are compared with experimental results of HNF combustion. It is shown that the low-activation-energy approach yields better agreement with experimental observations, for example, regression rate and temperature sensitivity, than the high-activation-energy approach.

Nomenclature

A = Arrhenius prefactor
a = burn rate coefficient
B = Arrhenius prefactor
c_p = specific heat capacity
D_g = Damkohler number, $k_g B_g p^2 M^2/[(m_{\text{ref}}R)^2 c_p]$
d = diffusion coefficient
E = activation energy
E^* = $E/[R(T_f - T_0)]$
f_r = fraction of Q_r absorbed below surface reaction zone, $\exp(-K_a x_R)$
J = $Q_r/[c_p m(T_s - T_0)]$
K_a = absorption coefficient
k = thermal conductivity
Le = Lewis number
M = molecular weight
m = mass flow rate
m^* = m/m_{ref}
n = pressure exponent
p = pressure
Q = heat release
Q_r = radiant heat flux
Q^* = $Q/[c_p(T_f - T_0)]$
R = universal gas constant
r_b = hydrazinium nitroformate regression rate
T = temperature
T^* = $T/(T_f - T_0)$
x = space coordinate
x_R = reaction zone length scale, $[k_c/(\rho_c c_p r_b)]/[E_c/(2RT_s)]$
x^* = $x/[k_g/(m_{\text{ref}}c_p)]$
Y = mass fraction
α = thermal diffusivity
δ = reaction order
ϵ = chemical reactivity
ρ = density

Subscripts and Superscripts

c = condensed phase
f = final
g = gas phase
ref = reference value
s = surface
0 = initial
$*$ = nondimensional parameter

Received 4 February 1998; revision received 23 September 1999; accepted for publication 25 September 1999.

*Ph.D. Student, P.O. Box 45, Research Group Rocket Technology; louwers@pml.tno.nl.
†Research Scientist, Research Group Rocket Technology.
‡Professor of Mechanical Engineering, Department of Mechanical and Industrial Engineering.
§Technical Staff Member, High Explosives Science and Technology Group.
¶Research Chemist, Weapons Division, Research Department.

Introduction

THE modeling of solid propellants may be a cost effective way to determine properties such as regression rates and temperature sensitivity before carrying out any experiments. Composite propellants are contemporary workhorses for many applications, but modeling of these heterogeneous propellants is very complex. Some models for composite propellant combustion have been developed, such as the Petite Ensemble Model.[1] However, these models require extensive experimental calibration.

Therefore, it is currently recognized that more complex models are needed to be able to compute regression rates and other properties a priori. As starting point for composite propellant models, many models of solid monopropellant combustion have been recently developed.[2–4] These models are often based on simplified chemical kinetics, coupled with a multiphase one-dimensional space domain. Because of the size of these numeric experiments, basic principles are often not revealed.

In this paper, modeling results using simplified approaches are presented. The goal in making the models is maximal predictive capability and accuracy, coupled with minimal complexity. This is achieved by using essential physics and chemistry only, yielding tractable models. The condensed phase is treated by a

high-activation-energy approximation method. The gas phase is treated in two ways: the classical high-activation-energy limit [Denison–Baum[5] and Williams[6] (DBW) model] and the recently introduced low-activation-energy limit [Ward et al.[7] Ward–Son–Brewster (WSB), model]. Both limits allow for an analytical solution of the gas-phase energy equation. The WSB approach was found to match the experimental observations much better than the DBW models for HMX and double-base propellants.[8]

It is the intention of this work to verify whether the new WSB approach also gives better results for hydrazinium nitroformate (HNF) combustion. HNF is a new chlorine-free oxidizer that is currently being studied for possible use in future generation composite propellants.[9] Neat HNF shows self-sustained combustion at pressures above 0.025 MPa (Refs. 10–12).

Model

The combustion of HNF is modeled as a one-dimensional, steady-state process. The condensed phase is described by a unimolecular, irreversible, zero-order decomposition reaction

$$A \rightarrow B \tag{1}$$

where A is the solid HNF and B some kind of unstable intermediate species (such as the observed NO_2, HONO, and N_2O). B reacts further according to the following bimolecular, irreversible, gas-phase reaction:

$$B + M \rightarrow C + M \tag{2}$$

where C are intermediate gas-phase products, such as NO. M are unstable species such as N, H, and OH. The kinetic scheme represented by Eqs. (1) and (2) is an ad hoc global description. This model was not derived from a detailed kinetic scheme, but from a conceptual point of view. The aforementioned species represented by B and C are representative for HNF and help to clarify the idea behind the global description.

The reactions represented by the second step ($B + M \rightarrow C + M$) consume the intermediate radical species. These reactions are characterized by high exothermicity and a low-activation-energy barrier. M may be viewed as a pool of unspecified chain carriers, whose mass fraction is constant, and as negligibly small compared to the main species B and C (Ref. 7). The reaction is second order overall, and first order with respect to B. For the purposes of modeling species conservation, no distinction is made between the M species that appear on the left- and right-hand sides of Eq. (2). The process is assumed to be a bimolecular exchange reaction, which for species bookkeeping purposes assumes only two gas species: B (reactant) and C (product). The preceding interpretation relates to the WSB model. For the DBW model, the kinetic interpretation is one of a gas-phase thermal decomposition, and M is interpreted in the usual sense, as any species.

The molecular weights of the various species are assumed to be equal, and mass diffusion in the gas phase is assumed to be described by Fick's law. The specific heat capacity and thermal conductivities are assumed to be constant. The gas-phase and the condensed-phase specific heat capacities are assumed to be equal. To simplify the solution of the gas-phase equations, the Lewis number is assumed to be unity, $Le = k_g/\rho_g d c_p = 1$. The propellant may be illuminated with an external laser heat flux, with radiative energy Q_r (watt per square meter). This heat flux is absorbed in the condensed phase according to Beer's law (absorption coefficient K_a). The gas-phase laser flux absorption is assumed to be zero. The gas phase is assumed to obey the ideal gas law. Mass diffusion in the condensed phase is neglected.

Condensed Phase

With the preceding assumptions, the condensed phase is described by the following energy equation:

$$mc_p \frac{\mathrm{d}T}{\mathrm{d}x} = k_c \frac{\mathrm{d}^2 T}{\mathrm{d}x^2} + Q_c \epsilon_c + Q_r K_a \exp(K_a x) \tag{3}$$

with boundary conditions

$$T(0) = T_s, \qquad \lim_{x \rightarrow -\infty} T(x) = T_0 \tag{4}$$

Inasmuch as a zero-order condensed-phase reaction was assumed, the reaction rate is given by

$$\epsilon_c = \rho_c A_c \exp[-(E_c/RT)] \tag{5}$$

It was shown by Von Elbe et al.[13] and Louwers et al.[12] that the condensed phase of HNF has a thin reactive zone, that is, a high activation energy for the decomposition process as given by Eq. (1). This means that activation energy asymptotics (AEA) may be used to find the solution of Eq. (3). The well-known solution is[14,15]

$$m^2 = \frac{A_c R T_s^2 k_c \rho_c \exp(-E_c/RT_s)}{E_c[c_p(T_s - T_0) - Q_c/2 - f_r Q_r/m]} \tag{6}$$

Gas Phase

Solution of the gas-phase equations is less straightforward. Most early models are based on the flame sheet approach, that is, a very thin reactive zone, where all of the gas-phase heat release occurs. This process is typical for gas-phase kinetics with high activation energy ($E_g \rightarrow \infty$). Mathematically the heat release can be approximated by a Dirac delta function.[16] It was recently argued by Ward et al. that a very low gas-phase activation energy ($E_g \rightarrow 0$) is more physical.[7] Their perspective is based on that the temperature profile of HMX could be much better replicated by $E_g = 0$ than by $E_g = \infty$. Analogs in gas-phase combustion provide further evidence that such an approach is not unrealistic. Most of the energy of a hydrogen/oxygen system is released during the recombination/termination step, which has a low-activation-energy barrier.[17] Both limit cases ($E_g = 0$ and $E_g = \infty$) will be discussed to see the overall effect on the model.

The energy equation in the gas-phase is

$$mc_p \frac{\mathrm{d}T}{\mathrm{d}x} = k_g \frac{\mathrm{d}^2 T}{\mathrm{d}x^2} + Q_g \epsilon_g \tag{7}$$

with the reaction rate given by

$$\epsilon_g = \rho_g^2 B_g Y T^2 \exp[-(E_g/RT)] \tag{8}$$

where Y is the mass fraction of B. The density of the gas phase ρ_g is found from the ideal gas law. The interface conditions are found from energy conservation at the surface

$$T_s = T_0 + \frac{Q_c}{c_p} + \frac{1}{mc_p}\left[k_g \left(\frac{\mathrm{d}T}{\mathrm{d}x}\right)_{x=0} + Q_r\right] \tag{9}$$

and

$$T_f = T_0 + \frac{Q_c + Q_g + Q_r/m}{c_p} \tag{10}$$

The species equation of the gas phase is

$$m \frac{\mathrm{d}Y}{\mathrm{d}x} = \rho_g d \frac{\mathrm{d}^2 Y}{\mathrm{d}x^2} - \epsilon_g \tag{11}$$

For the species equation, the boundary conditions are

$$Y_s = 1 + \frac{\rho_g d}{m}\left(\frac{\mathrm{d}Y}{\mathrm{d}x}\right)_{x=0} \tag{12}$$

and

$$\lim_{x \rightarrow \infty} Y = 0 \tag{13}$$

Because of the assumption $Le = 1$, the gas-phase energy equation and species equation are uncoupled and can be written as two similar

nondimensional equations (nondimensional quantities are denoted by *)[7]

$$m^* \frac{\mathrm{d}T^*}{\mathrm{d}x^*} = \frac{\mathrm{d}^2 T^*}{\mathrm{d}x^{*2}} - D_g \left(T_f^* - T^*\right) \exp\left(-\frac{E_g^*}{T^*}\right) \tag{14}$$

and

$$m^* \frac{\mathrm{d}Y}{\mathrm{d}x^*} = \frac{\mathrm{d}^2 Y}{\mathrm{d}x^{*2}} - D_g Y \exp\left(-\frac{E_g^*}{T_f^* - Y Q_g^*}\right) \tag{15}$$

The boundary equations transform accordingly. For arbitrary values of E_g^*, Eq. (14) has to be solved iteratively with Eq. (6) to yield T_s^* and m^*. Note that solution of this set requires solution of a second-order differential equation. For the two limiting cases, $E_g = 0$ and $E_g \to \infty$, it is possible to obtain an analytical solution.

The first limit is that of a very low activation energy in the gas phase, $E_g \to 0$. For this case an analytical solution of Eq. (14) can be obtained,

$$\frac{T^* - T_f^*}{T_s^* - T_f^*} = \exp\left(-\frac{x^*}{x_g^*}\right) \tag{16}$$

In Eq. (16) x_g^* is a dimensionless characteristic gas reaction zone thickness given by

$$x_g^* = \frac{2}{\sqrt{m^{*2} + 4D_g} - m^*} \tag{17}$$

Using different approximations, Miller derived similar results for the gas phase.[18] In Miller's work the gas phase reaction is described by a first-order reaction and a constant temperature reaction rate. Because M is assumed constant in this work, reaction (2) is in essence also first order. The constant temperature reaction rate approximation corresponds with a constant, temperature-independent, reaction rate, that is, $E_g = 0$.

In summary, in the limit of a high condensed-phase activation energy, coupled with a low-activation-energy gas phase, the analytical solution of the problem is given by the (nondimensional) form of Eq. (6),

$$m^{*2} = \frac{A_c^* T_s^{2*} \exp\left(-E_c^*/T_s^*\right)}{E_c^* \left(T_s^* - T_0^* - Q_c^*/2 - f_r J\right)} \tag{18}$$

This equation is solved simultaneously with Eq. (17) The energy balance is given by the nondimensional result of Eq. (9),

$$T_s^* = T_0^* + Q_c^* + \frac{Q_g^*}{x_g^* m^* + 1} \tag{19}$$

For the high-activation-energy gas phase ($E_g \to \infty$), the regression rate is given by Ibiricu Williams's[14] gas-phase controlled analytical solution (for $E_g/RT_f \gg 1$)

$$m^2 = \frac{2k_g B_g M^2 p^2 c_p T_f^4}{E_g^2 Q_g^2} \exp\left(-\frac{E_g}{RT_f}\right) \tag{20}$$

This expression indicates that the mass flux is determined by gas kinetics only and not by decomposition kinetics. Note that actually Q_r affects T_f [Eq. (10)], which affects m. For this case, the energy balance yields

$$T_s^* = T_0^* + Q_c^* + Q_g^* \exp\left(-x_g^* m^*\right) \tag{21}$$

For the high-activation-energy limit case, the AEA result [Eq. (18)] is still used for the determination of the surface temperature T_s^*. Results of this traditional analytical limit case will be compared with the new concept of $E_g = 0$ to show the overall improvements of the model's predictive capability.

Results

The properties of HNF as used for the calculations are summarized in Table 1. During all calculations these values are held constant. The condensed-phase activation energy $E_c = 75$ kJ/mol was found to give good results in the whole pressure range of interest. This value is close to the 84 kJ/mol required to break up HNF into liquid hydrazine and nitroform. The values of the Arrhenius prefactors, A_c and B_g, were determined from the experimental observation that $T_s = 523$ K (Ref. 12) and $r_b = 0.77$ mm/s at 0.1 MPa (Refs. 10–12). After this calibration of the model at a single burning condition, the regression rate is calculated at different pressures, without modification of any of the other parameters. The density of the pressed HNF pellets was 1740 kg/m^3 (Ref. 12). The thermophysical properties of solid HNF were recently measured.[19] The specific heat capacity and thermal conductivity were found to have a slight temperature dependence. However, thermal conductivity was found to decrease near the burning surface, due to cracks during combustion.[20] In this model constant values at 100°C are used.

Steady-State HNF Combustion

Figure 1 shows the results of the calculated regression rate for both models, compared with experimental data (from Ref. 21). Like most energetic materials, HNF's regression rate can be described by $r_b = ap^n$. The high-activation-energy limit yields the familiar $n = \delta/2 = 1$, whereas $n = 0.89$ was found experimentally for HNF combustion (least-squares fit to all data points in Fig. 1). Because the regression rate was gauged at 0.1 MPa, the flame sheet overpredicts the regression rates above 0.1 MPa. The WSB approach shows good agreement with the experimental results. This model predicts $n = 0.87$ (at 1 MPa).

However, above 0.7 MPa, there is a clear difference between the WSB results and the experimental data. This difference can be because not only the gas-phase kinetics change with pressure, but also the flame temperature. At 0.1 MPa the flame temperature of HNF is $T_f = 2766$ K. When the pressure is increased, the flame temperature of HNF increases considerably, for example, $T_f = 2949$ K at

Table 1 Input values used for HNF calculations

Parameter	Value	Unit
Q_g	2429	kJ/kg
Q_c	−30.0	kJ/kg
A_c	1.67×10^9	1/s
B_g		
$E_g = 0$	4.45×10^{-2}	m^3/kg K^2 s
$E_g = \infty$	1.06×10^4	m^3/kg K^2 s
c_p	0.97	kJ/kg K
k_g	0.054	W/mK
k_s	0.15	W/mK
E_c	75	kJ/mol
E_g	167	kJ/mol
ρ_c	1740	kg/m^3
M	25.6	kg/kmol

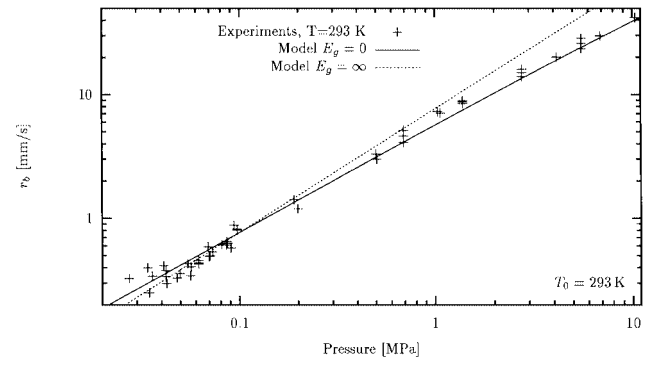

Fig. 1 Comparison of calculated and measured regression rate of neat HNF samples.

Table 2 Final flame temperature T_f and most important species concentrations (mole fractions) of neat HNF combustion[a]

p, MPa	T_f, K	H	H_2	O	O_2	OH	CO	CO_2	N_2	NO	H_2O
0.01	2578	0.017	0.023	0.022	0.113	0.048	0.047	0.090	0.338	0.014	0.288
0.1	2766	0.010	0.018	0.016	0.108	0.046	0.040	0.100	0.342	0.017	0.304
1	2949	0.005	0.012	0.010	0.103	0.041	0.030	0.112	0.345	0.021	0.321
10	3112	0.002	0.007	0.005	0.099	0.033	0.019	0.125	0.349	0.025	0.337
100	3237	0.001	0.003	0.002	0.095	0.024	0.010	0.136	0.351	0.028	0.349

[a]Results from NASA SP-273 chemical equilibrium[22] calculations.

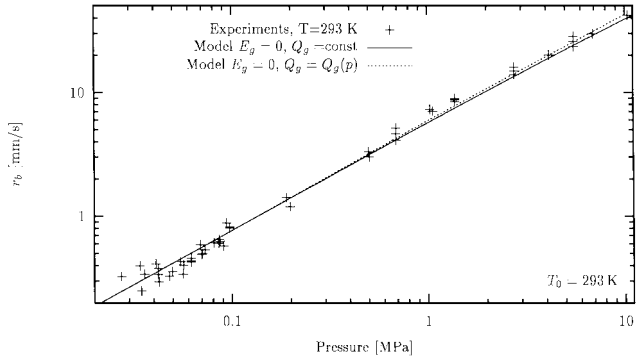

Fig. 2 Effect of introducing pressure dependent Q_g to account for the varying flame temperature with pressure.

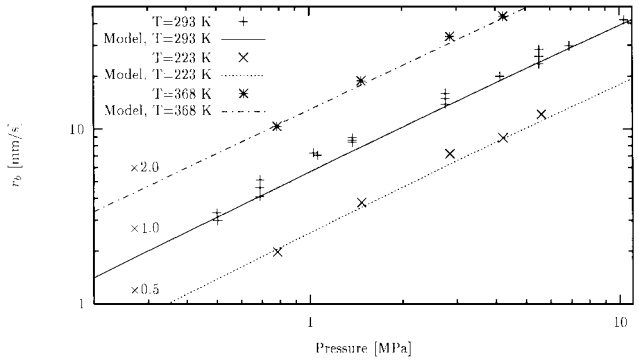

Fig. 3 Comparison of calculated (WSB-model) and measured regression rate of neat HNF samples. (Note the multiplication factors that are introduced to prevent overlap of data.)

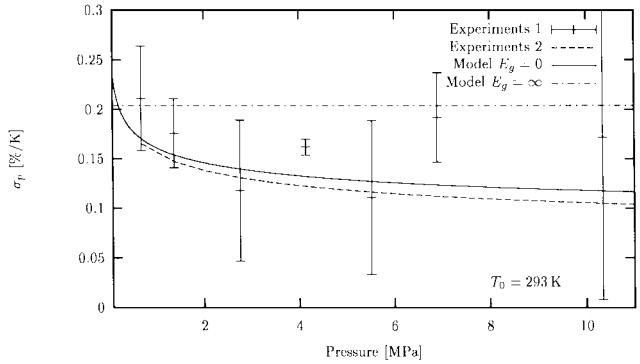

Fig. 4 Experimental vs theoretical temperature sensitivity of HNF for both modeling approaches; error bars indicate the standard deviation from the $\ln(r_b)$ vs T fit.

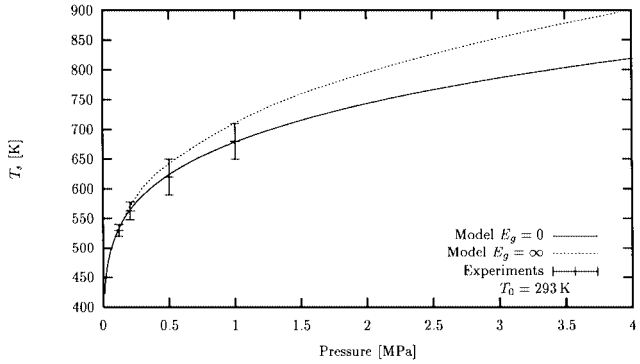

Fig. 5 Experimental and predicted surface temperature.

1 MPa and $T_f = 3112$ K at 10 MPa. This is because the equilibrium composition is dependent on the pressure (see Table 2).[22] The higher flame temperature results in an extra heat feedback to the surface not accounted for by the model. This varying flame temperature can be introduced into the model by varying Q_g as function of pressure, so that the calculated adiabatic flame temperature is reached, $T_f = (Q_g + Q_c)/c_p + T_0$. The rest of the parameters are kept constant. The result is improved agreement between the WSB model and the experimental results (see Fig. 2). For simplicity, this modification of the model will not be used throughout the rest of this paper, and from now on, constant Q_g values will be used.

Also, for low and high initial temperatures, the WSB model has good agreement with the experimental results (see Fig. 3). This sensitivity of the burning rate to the initial temperature is defined by the following expression:

$$\sigma_p = \frac{1}{r_b}\left(\frac{\partial r_b}{\partial T_0}\right)_p \tag{22}$$

By determining the regression rate at 292 and 293 K, HNF's temperature sensitivity was determined for both the DBW and the WSB models (see Fig. 4). This graph also shows the experimental determined temperature sensitivity from the data points of Fig. 3. This is done in two ways: The first is direct determination of σ_p at each pressure by a fit of $\ln(r_b)$ vs temperature. The second method is by a least-squares power laws fit to the regression rate curves at each pressure. Then the temperature sensitivity is determined from the differences between these fits at each pressure. If the propellant burns nicely according to $r_b = ap^n$, then the second method will give more accurate results.

From Fig. 4 it is seen that the low-activation-energy limit predicts a pressure dependence of the temperature sensitivity. This limit case shows reasonable agreement with the direct determined values for σ_p. The agreement with the temperature sensitivity as determined by the second method is very good. The $E_g \to \infty$ model is not capable of capturing a pressure variation of σ_p. Within the $E_g \to \infty$ approach, only a constant temperature sensitivity is calculated, $\sigma_p = (T_f + E_g/2RT_f)/T_f$. Unfortunately, the large errors from the direct method make it impossible to favor one of the two modeling approaches. The temperature sensitivity as determined from fitting the power laws first is much better for the WSB approach than for the DBW model.

The variation of the surface temperature T_s with pressure is shown in Fig. 5. Although both models share the same condensed-phase equations, the predicted surface temperatures are different because each model predicts a different mass flux for each pressure. Figure 5 also shows some experimental results that were obtained with 5-μm ribbon thermocouples.[12] The results show good agreement with the

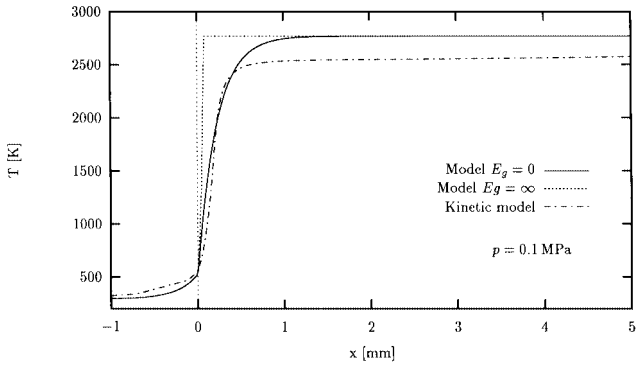

Fig. 6 Temperature profile of HNF for both limit models and a comprehensive detailed kinetical model.

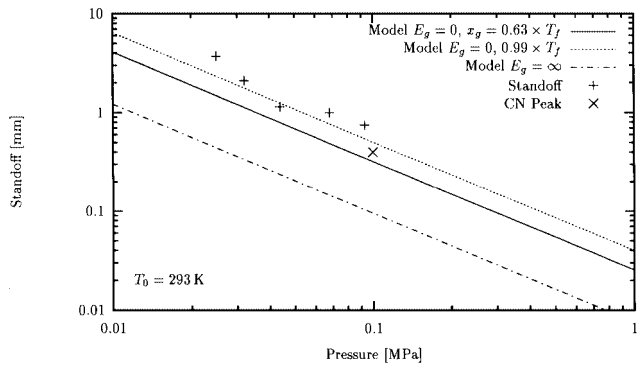

Fig. 7 Flame standoff distance as calculated from both models, compared with experimental determined flame standoff (height above the burning surface of CN chemiluminiscence) and CN profile peak position as determined by PLIF.

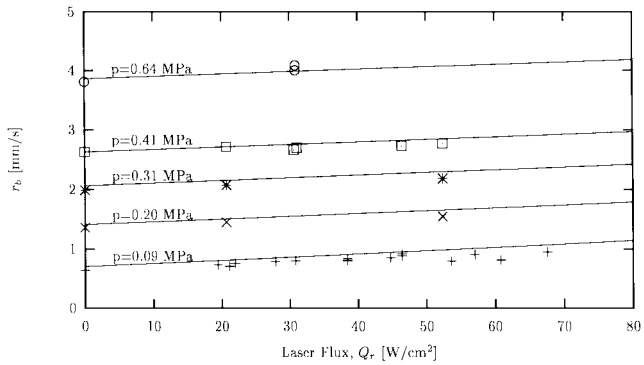

Fig. 8 Laser-assisted regression rates of HNF at different pressures, where points are experimental data and solid lines are WSB model's results for K_a = 1000 cm^{-1}. WSB model predicts HNF's sensitivity to an external heat source accurately for all pressures.

WSB model. These results support the validity of the AEA result [Eq. (6)].

Recently, a kinetical model for HNF combustion was developed.[23] This model belongs to the group of numerical models mentioned in the Introduction. The solid to gas interface is fixed at the origin by specification of the surface temperature. This then yields the mass flux as an eigenvalue of the system of governing equations.[3] A limited set of global decomposition reactions is allowed to take place in the condensed phase. The gas phase is modeled by Yetter's RDX gas-phase mechanism[24] with added reactions for HNF decomposition. Typical products formed at the surface are $HNF_{(g)}$, CO, N_2O, HONO, and N_2H_4.

Figure 6 compares the temperature profile as found from both limit cases and the detailed modeling. It may be seen that the temperature profile of the simplified WSB model is close to that of the detailed chemical model. Both simplified models show a temperature profile close to the final flame temperature at $x = 1$ mm. The detailed calculations show a lower temperature due to the slow NO reactions, similar to the dark zone in double-base propellants. With a second step in the gas phase, $C \rightarrow D$, the simple models would also be able to calculate this intermediate zone. The final flame temperature of the kinetical model is equal to that of the other models. It was determined by NO UV-absorption experiments that temperatures close to the adiabatic flame temperature are reached within 1 mm above the surface. All three modeling approaches confirm this. However, the accuracy of the absorption experiments does not allow rejection of one of the models.

A closer agreement between the temperature profile of WSB/DBW models and the kinetic model is obtained by using the intermediate temperature of 2550 K as the final temperature. It was verified that after recalibration of the WSB model the effect is small. For the DBW model, there is no effect, as a decrease of Q_g is compensated for by a decrease of B_g [see Eq. (20)]. These results will, therefore, not be discussed here.

Figure 7 shows the position where 63%($=x_g$) and 99% of the final flame temperatures are reached. These positions are characteristic dimensions for the gas-phase reaction zone thickness. In Fig. 7, this flame thickness is compared to several experimental results. The flame standoff distances in Fig. 7 were obtained from video images as the distance off the surface of the CN chemiluminiscent emission. The CN profile peak location was determined by planar laser-induced fluorescence (PLIF), which is a more accurate determination of the CN standoff. The CN profile peaks do not necessarily coincide with x_g, but should at least follow the same trend and be of the same order of magnitude. The magnitude is much better predicted by the WSB model. The DBW-model flame thickness is an order of magnitude too thin (as also the case for HMX). It is seen that both the DBW and WSB models predict the experimental observed pressure dependence (nearly $1/p$).

Laser-Assisted Combustion

As part of the study of the transient combustion of HNF, Finlinson determined the laser-assisted regression rates of HNF.[10,11] During combustion the laser energy is absorbed in the condensed phase near the burning surface and increases the regression rate. An infrared 10.6-μm CO_2 laser was used in Finlinson's study.[11] The laser-assisted regression rate data allows further validation of the model. The absorption coefficient for the CO_2 wavelength has been estimated to $K_a \sim 1000$ cm^{-1} (Ref. 20). No absorption or reflection measurements have been carried out for HNF in the 10.6-μm CO_2-laser range used by Finlinson.[11] The reflection coefficient is determined from a best fit to all experimental data. From the preceding section, it has become clear that the low-activation-energy limit, WSB, shows the best agreement with the experiments. Therefore, only this model will be discussed.

Figure 8 shows the laser-assisted combustion of HNF. For all pressures the models predict the sensitivity to the external laser heat flux to be in good agreement with the experimental data. The difference between the experiments and the modeling is caused by the small inaccuracies of the model, already at $Q_r = 0$. For these calculations a surface reflection of 60% was used. This value is comparable to the values used for HMX modeling.[25] This work indicates a surface reflectivity of 50%. Neat HMX samples show only 15% reflectivity at room temperature. Several explanations for this difference can be given: ions present in the melt layer, enhanced scattering inside the melt layer due to bubbles, or enhanced absorption at the burning surface due to the presence of decomposition products (hence, increased reflectivity). If the pressure increases, then the melt thickness decreases. This implies a lower reflection. The measurements at 0.6 MPa seem to indicate this. However, the number of measurements at this pressure is limited.

Conclusions

Two very simple models for the combustion of HNF have been presented. The gas phase has been calculated by two limit approaches: low (WSB) and high (DBW) gas-phase activation energy.

The WSB approach shows great predictive capability in both laser-assisted and self-sustained regression rates, in temperature sensitivity, and in surface temperatures. The agreement of these propellant properties is much better than with the usual assumption of large gas-phase activation energy (DBW). By introducing HNF's strong pressure-dependent adiabatic flame temperature into the WSB-model, even better results are obtained.

Acknowledgments

S. F. Son is sponsored by Los Alamos National Laboratory, which is supported by the U.S. Department of Energy under Contract W-7405-ENG-36. T. Parr and D. Hanson-Parr are sponsored under Contract N0001495WX20018 with the Office of Naval Research, Scientific Officer Richard Miller. The authors would like to thank Jerry Finlinson from the U.S. Naval Air Warfare Center, China Lake, for providing experimental data and helpful discussions.

References

[1]Glick, R. L., "On Statistical Analysis of Composite Solid Propellant Combustion," *AIAA Journal*, Vol. 12, No. 3, 1974, pp. 384, 385.

[2]Liau, Y. C., and Yang, V., "Analysis of RDX Monopropellant Combustion with Two-Phase Subsurface Reactions," *Journal of Propulsion and Power*, Vol. 11, No. 4, 1995, pp. 729–739.

[3]Prasad, K., Yetter, R. A., and Smooke, M. D., "An Eigenvalue Method for Computing the Burning Rates of RDX Propellants," *Combustion Science and Technology*, Vol. 124, Nos. 1–6, 1997, pp. 35–82.

[4]Davidson, J., and Beckstead, M., "Improvements to RDX Combustion Modeling," 34th Aerospace Sciences Meeting and Exhibit, Reno, NV, Jan. 1996.

[5]Denison, M. R., and Baum, E., "A Simplified Model of Unstable Burning in Solid Propellants," *ARS Journal*, Vol. 31, Aug. 1961, pp. 1112–1122.

[6]Williams, F. A., "Quasi-Steady, Gas-Phase Flame Theory in Unsteady Burning of a Homogeneous Solid Propellant," *AIAA Journal*, Vol. 11, No. 9, 1973, pp. 1328–1330.

[7]Ward, M. J., Son, S. F., and Brewster, M. Q., "Steady Deflagration of HMX with Simple Kinetics: A Gas Phase Chain Reaction Model," *Combustion and Flame*, Vol. 114, Nos. 3, 4, 1998, pp. 556–568.

[8]Brewster, M. Q., Ward, M. J., and Son, S. F., "New Paradigm for Simplified Combustion Modeling of Energetic Solids: Branched Chain Gas Reaction," AIAA Paper 97-3333, 1997.

[9]Schöyer, H. F. R., Schnorhk, A. J., Korting, P. A. O. G., van Lit, P. J., Mul, J. M., Gadiot, G. M. H. J. L., and Meulenbrugge, J. J., "Development of Hydrazinium Nitroformate Based Solid Propellants," *Journal of Propulsion and Power*, Vol. 11, 1995, pp. 856–859.

[10]Finlinson, J. C., and Atwood, A. I., "HNF Burnrate, Temperature Sensitivity, and Laser Recoil Response from 1 to 6 atm," 34th JANNAF Combustion Meeting, West Palm Beach, FL, Oct. 1997.

[11]Finlinson, J. C., "Laser Recoil Combustion Response of HNF Oxidizer from 1 to 6 atm," AIAA Paper 97-3342, 1997.

[12]Louwers, J., Gadiot, G. M. H. J. L., Versluis, M. J., Landman, A. J., van der Meer, T. H., and Roekaerts, D., "Combustion of Hydrazinium Nitroformate Based Compositions," AIAA Paper 98-3385, 1998.

[13]von Elbe, G., Friedman, R., Levy, J. B., and Adams, S. J., "Research on Combustion in Solid Rocket Propellants: Hydrazine Nitroform as a Propellant Ingredient," Atlantic Research Corp., TR DA-36-034-AMC-0091R, 1964.

[14]Lengelle, G., "Thermal Degradation Kinetics and Surface Pyrolysis of Vinyl Polymers," *AIAA Journal*, Vol. 8, No. 11, 1970, pp. 1989–1998.

[15]Ibiricu, M. M., and Williams, F. A., "Influence of Externally Applied Thermal Radiation on the Burning Rates of Homogeneous Solid Propellants," *Combustion and Flame*, Vol. 24, Feb.–June 1975, pp. 185–198.

[16]Buckmaster, J. D., "An Introduction to Combustion Theory," *The Mathematics of Combustion*, Frontiers in Applied Mathematics, Society for Industrial and Applied Mathematics, Philadelphia, PA, 1985, pp. 3–46.

[17]Zeldovich, Y. B., "Chain Reactions in Hot Flames—an Approximate Theory of Flame Velocities," *Kinetika i Kataliz*, Vol. 2, 1961, pp. 305–318.

[18]Miller, M. S., "In Search of an Idealized Model of Homogeneous Solid Propellant Combustion," *Combustion and Flame*, Vol. 46, Nos. 1, 2, 1982, pp. 51–73.

[19]Hanson-Parr, D., and Parr, T. P., "Measurements of Solid Rocket Propellant Oxidizers and Binder Materials as a Function of Temperature," *Journal of Energetic Materials*, Vol. 17, 1999, pp. 001–047 (submitted for publication).

[20]Louwers, J., Gadiot, G. M. H. J. L., Versluis, M., Landman, A. J., van der Meer, T. H., and Roekaerts, D., "Measurement of Steady and Non-Steady Regression Rates of Hydrazinium Nitroformate with Ultrasound," *International Workshop on Measurement of Thermophysical and Ballistic Properties of Energetic Materials*, Politecnico di Milano, Milano, Italy, June 1998.

[21]Atwood, A. I., Boggs, T. L., Curran, P. O., Parr, T. P., Hanson-Parr, D., Wiknich, J., and Price, C. F., "Burn Rate Temperature and Pressure Sensitivity of Solid Propellant Ingredients," *International Workshop Combustion Instability of Solid Propellants and Rocket Motors,* Politecnico di Milano, Italy, June 1997.

[22]Gordon, S., and McBride, B. J., "Computer Code for Calculation of Complex Chemical Equilibrium Compositions, Rocket Performance, Incident and Reflected Shocks, and Chapman–Jouguet Detonations," NASA Technical Rept. SP-273, interim revision, 1976.

[23]Louwers, J., "A Model for HNF Monopropellant Combustion: First Results," TNO Prins Maurits Lab., Rept. PML 1996-C92, Rijswijk, The Netherlands, 1996.

[24]Yetter, R. A., Dryer, F. L., Allen, M. T., and Gatto, J. L, "Development of Gas-Phase Reaction Mechanisms for Nitramine Combustion," *Journal of Propulsion and Power*, Vol. 11, 1995, pp. 683–697.

[25]Loner, P. S., and Brewster, M. Q., "On the Oscillatory Laser-Augmented Combustion of HMX," *Proceedings of the 27th International Symposium on Combustion*, The Combustion Institute, Pittsburgh, PA, 1998, pp. 2309–2317.